NANO · MICRO small
www.small-journal.com

Multicolor 3D Orbital Tracking

*Frank Mieskes, Evelyn Ploetz, Fabian Wehnekamp, Virgile Rat, and Don C. Lamb**

Feedback-based single-particle tracking (SPT) is a powerful technique for investigating particle behavior with very high spatiotemporal resolution. The ability to follow different species and their interactions independently adds a new dimension to the information available from SPT. However, only a few approaches have been expanded to multiple colors and no method is currently available that can follow two differently labeled biomolecules in 4 dimensions independently. In this proof-of-concept paper, the new modalities available when performing 3D orbital tracking with a second detection channel are demonstrated. First, dual-color tracking experiments are described studying independently diffusing particles of different types. For interacting particles where their motion is correlated, a second modality is implemented where a particle is tracked in one channel and the position of the second fluorescence species is monitored in the other channel. As a third modality, 3D orbital tracking is performed in one channel while monitoring its spectral signature in a second channel. This last modality is used to successfully readout accurate Förster Resonance Energy Transfer (FRET) values over time while tracking a mobile particle.

1. Introduction

Since the first publication of a single-particle tracking (SPT) instrument for tracking biological samples in 1971 by Berg,[1] the field of SPT approaches has tremendously grown. Today, SPT is typically split into two approaches: camera-based measurements where movies are collected and trajectories extracted afterward, and real-time techniques using active feedback loops. In post-processing approaches, the lateral information of the particle is directly encoded in the pixels covering the field of view (FOV). The axial position of the emitter can be obtained by recording images of several planes (z-stacking),[2] imaging the diffraction pattern of out-of-focus particles,[3] or by engineering the point spread function (PSF).[4,5] In the case of 3D active feedback tracking, popular approaches include tetrahedral detection,[6] TSUNAMI,[7] 3D-SMART,[8] and (PIE-)MinFLUX.[9,10] Real-time tracking approaches are low throughput but have the advantage of typically higher temporal resolution and the ability to follow a single particle over longer periods of time. As the microscope system is directly focused on the particle of interest, more advanced spectroscopic information can also be collected on the particle during tracking.[11] This enables more elaborate analyses of the tracked particle and its measured motion.[12]

In this paper, we focus on orbital tracking, which was proposed theoretically for two dimensions by Jörg Enderlein in 2000[13] and realized experimentally in three dimensions by Enrico Gratton.[14] In orbital tracking, the excitation laser is rotated in a circular pattern or "orbit" around the tracked object. This real-time SPT approach combines high spatial resolution (*xy*: ≈3 nm; *z*: ≈20 nm) with fast response times (≈5 ms) over large distances (>100 µm) and time ranges (up to 10 min). In combination with photoactivation, this method provides unique insights into biological systems, e.g., by tracking cargo transport in vivo or mitochondrial trafficking in zebrafish larvae,[12,15] measuring the metabolism in lysosomes by detecting solvent-dependent intensity fluctuations[16] or monitoring heterogeneities on surfaces.[17] Furthermore, slow conformational changes can be probed in solution, which are not accessible by conventional fluorescence correlation spectroscopy while tracking.[18]

Single-particle tracking provides super-resolution information in living dynamic systems. However, often not only subdiffractional resolution is required, but a methodology that additionally allows for investigating the interaction of two particles with high temporal and spatial resolution. This requires the existence of a second channel for SPT and the capability of synchronized tracking. While dual-color SPT is relatively straightforward for camera-based approaches,[19–21] feedback-based, dual-color SPT methods have only been developed to track particles in close vicinity (<500 nm) or read out the spectral properties during tracking. Using two-photon excitation, Gratton and

F. Mieskes, E. Ploetz, F. Wehnekamp, V. Rat, D. C. Lamb
Department of Chemistry and Center for NanoScience (CeNS)
Ludwig-Maximilians-Universität München
Butenandtstraße 11, 81377 Munich, Germany
E-mail: d.lamb@lmu.de

F. Mieskes, E. Ploetz, F. Wehnekamp, V. Rat, D. C. Lamb
Nanosystems Initiative Munich (NIM)
Ludwig-Maximilians-Universität München
Schellingstraße 4, 80799 Munich, Germany

F. Mieskes, E. Ploetz, F. Wehnekamp, V. Rat, D. C. Lamb
Center for Integrated Protein Science Munich (CiPSM)
Ludwig-Maximilians-Universität München
Butenandtstraße 5–13, 81377 Munich, Germany

The ORCID identification number(s) for the author(s) of this article can be found under https://doi.org/10.1002/smll.202204726.

DOI: 10.1002/smll.202204726

co-workers demonstrated spectra collection while performing orbital tracking[11] and have shown that distances between two closely spaced particles can be measured with nm accuracy.[22] Liu et al. tracked conformational changes of tandem partners using two-photon excitation with the TSUNAMI approach.[23] Werner and co-workers extended their tetrahedral tracking technique by a second detection volume allowing for the measurement of apparent FRET during tracking.[24] In the later dual-color approach, the active tracking is carried out in the donor channel while probing the acceptor signal in parallel. However, none of these approaches have demonstrated the tracking of two particles independently nor of probing accurate FRET.

In this paper, we developed a 3D orbital-tracking system[12] for multi-color tracking: It allows for dual-channel tracking of independently as well as correlatively moving particles and provides multi-color detection to enable single-molecule spectroscopy of diffusing particles. First, individual beads emitting at different spectral ranges were tracked independently. A diffusion analysis of the individual 3D trajectories allows for characterization of the motion of particles and monitoring of particle interactions while diffusing in the medium. Here, the position and distance between the particles can be monitored in real time with nanometer resolution. In the next step, we demonstrate its capabilities by dual-color tracking of double-labeled beads in solution mimicking co-diffusive motion. Using two detectors per tracking channel in the presented 3D orbital tracking approach, we employ one detector pair for SPT while using the other detector pair to localize the second fluorescence signal. Alternatively, in a third approach, we use the second detection channel to perform single-molecule spectroscopy. In particular, we performed accurate, single-pair FRET (spFRET) measurements on diffusing particles. This allows us to monitor the position as well as the time trajectories of FRET efficiency of the freely moving particles simultaneously.

2. Experimental Section

2.1. Materials and Preparation Procedures

Chemicals were purchased from Sigma–Aldrich and used without further purification, if not stated otherwise, including bovine serum albumin (BSA), catalase (*Asp. niger*), ethylenediamine-tetraacetic acid (EDTA), glucose, glucose oxidase (*Asp. niger* Type VII), glycerol, phosphate-buffered saline (PBS), Tris base, Tris HCl, Trolox, and sodium chloride.

For image calibration experiments, multifluorescent beads purchased from Spherotec Inc (FP-0557-2) were used. For dual-color tracking experiments of independently moving beads, we used two suspensions of coated, fluorescently labeled polystyrene particles 0.1% (w/v) purchased from Kisker Biotech: 1) Streptavidin-coated particles (named "yellow"/PC-SAFY-0.5; Kisker) emitting between 460–540 nm and having an average diameter of 450 nm and 2) Avidin-coated particles (named "purple'/PC-AFU-0.5; Kisker) emitting between 580–650 nm with a diameter of 560 nm. For dual-color tracking measurements on co-diffusing labeled objects, the avidin-coated, 'purple" particles (PC-AFU-0.5; Kisker) were employed, and

```
          5'-GACCTATGCTAATTATTAACCCCTTAXATTCCTCGACGAC-3'-BIO
DNA 3:  3'-CTGGATACGATTAATAAYTGGGGAATATAAGGAGCTGCTG-5'
DNA 2:  3'-CTGGATACGATYAATAATTGGGGAATATAAGGAGCTGCTG-5'
DNA 1:  3'-CTGGAYACGATTAATAATTGGGGAATATAAGGAGCTGCTG-5'
X = T - Atto647N          Y = T - Atto565
```

Scheme 1. DNA sequences used in Tracking/spFRET experiments. The top strand (T) contained the donor fluorophore (Atto565), while one of three different bottom strands (B) containing the acceptor fluorophore (Atto647N) was annealed to the top strand.

they were labeled with a biotinylated Atto488-dye (AD 488; Atto-Tec GmbH). Dual-color surface localization experiments of the same bead samples were used for verification of the precision of the image calibration procedure (Figure 3B).

Tracking experiments with spFRET readout of dsDNA oligos were carried out on labeled streptavidin-coated silica beads (480 nm, CS01000-2; Polysciences Europe GmbH) with biotinylated dsDNA oligos and Atto488. Labeling as well as mixing of particles was carried out in PBS.

Single-stranded DNA 40-mers containing the desired modifications were obtained commercially (**Scheme 1**). Bottom strands were labeled at the B6, B12, and B18 positions with the donor fluorophore Atto565 and purchased from Metabion. The top strand was purchased from IBA, biotinylated at the 3′-end and contained the acceptor dye Atto647N at position T27. The complementary DNA strands were annealed in 500 mM NaCl, 20 mM TRIS, and 1 mM EDTA at pH 8. After heating the mixture to 95 °C, the temperature was held for 3 min and cooled down to 4 °C at a rate of 1 °C min^{-1}.

If not mentioned otherwise, all samples were measured in 8-well chamber slides (Nunc LabTek I, Thermofisher) that had been passivated with 1 mg mL^{-1} BSA in PBS for 10 min before the measurement. MFD-PIE experiments[25] were carried out on freely diffusing dsDNA molecules at 25–50 pM in PBS at room temperature (20 °C).

2.2. Cell Culture

An HuH7 cell line stably expressing Rab5-GFP had been validated and tested negative for mycoplasma contamination. HuH7 Rab5-GFP were cultured in high-glucose DMEM (Gibco) with 10% foetal bovine serum, 100 U mL^{-1} Penicillin, 100 µg mL^{-1} streptomycin, and 400 µg mL^{-1} geneticin (G418, Gibco) with 5% CO_2 at 37 °C. Cells were plated at 80,000 cells per well in a LabTek II chambered coverglass (Nunc, Thermofisher). Twenty-Four hours after seeding, the medium was exchanged with a DMEM red phenol free medium, and the previously described "purple" beads were added half an hour prior to the observation.

2.3. Orbital Tracking Setup

2.3.1. Instrument

The general microscope design was based on a previously developed confocal setup for one-color 3D Orbital-Tracking,[12] which was extended for multi-channel, dual-color tracking.

Three lasers were used as excitation sources (Sapphire 488-20 CDRH; Coherent/Jive CDRH CW 561; Cobolt/05-LHP-151; Melles Griot) at 488, 561, and 633 nm, respectively. The lasers were guided through an acousto-optical tunable filter (TF525-250-6-3-GH19A, Gooch & Housego) to control the excitation cycles of the three light sources. Afterwards, they were coupled into a single-mode fiber (QPMJ-A3A,3A-405/650-3/125-3-5-1; Oz Optics) to clean up the beam profile and decouple the excitation path from the microscope. The excitation and detection path of the microscope were combined by a quad-band polychroic mirror (zt405/488/561/640rpc; AHF), which transmits the fluorescence emission and reflects the laser beams onto a two-axis galvanometric mirror system (GVSM002/M; Thorlabs). A telescope system (80 and 250 mm achromatic lenses, Thorlabs) was used to image the output of the galvanometric mirrors unto the back aperture of the objective and the laser beam was focused by the objective onto the sample (PlanApo VC 60x/1.20WI; Nikon). The fluorescent signal was collected by the same objective. After passing the quad-band polychroic mirror, a long pass dichroic mirror (H560 LPXR, AHF) reflects the emission triggered by the 488 nm excitation laser. The fluorescence emission was filtered by an emission bandpass filter (525/50 Brightline HC; AHF) and then directed onto the two detection paths by a 50:50 beam splitter (#F21-020; AHF). Afterwards, it was focused by a lens (AC254-050-AB; Thorlabs) onto two 50 µm multimode fibers (M42L01, Thorlabs), which act as confocal pinholes, which guide the light to the separate avalanche photodiode detectors (APD, CountBlue; Laser Components).

The second detection channel was constructed identically. It shared the same geometry as channel one but employed two different focusing lenses (AC254-075-AB; Thorlabs) and APDs (SPCM-CD 3017; Perkin Elmer). For the dual-color tracking modality, the fluorescent signal was split onto two detectors by a 50:50 beam splitter (#F21-020; AHF) and spectrally filtered by an emission filter (685/70; Thorlabs). For parallel spectroscopic readout (in this case FRET), the 50:50 beam splitter was exchanged by a dichroic mirror (zt640rdc; Chroma) separating the donor from the acceptor signal. Each beam was cleaned up by an additional emission filter (593/40 and 685/70; Thorlabs, respectively).

2.3.2. Tracking Software

The experimental setup was controlled using a Field Programmable Gate Array (FPGA) controlled via LabVIEW2018. The software was executed on two different levels, consisting of a non-deterministic and a deterministic execution (**Figure 1**), to achieve exact hardware triggering during the orbital tracking experiment, as described previously.[12] In brief, the self-written program was executed on two systems: the host computer and a deterministic processing unit (cRIO 9082; National Instruments), combining a real-time processor and a FPGA. The real-time unit synchronizes all hardware components, executes the tracking algorithm, and streams the data to the host computer. It synchronizes, in particular, the execution of the hardware via TTL pulses, receives the incoming TTL signals from the detectors, and generates the voltages for repositioning the galvanometric mirrors to generate the rotating orbit of the exciting lasers. Each orbit was divided into 16 segments. The FPGA bins the photon detected for each orbit segment, stores it in a direct memory access first-in-first-out (DMA-FIFO) buffer, and streams it to the real-time processor for calculating the particle position within the orbit (see Section 2.3.3, Tracking algorithm). This was done for both detectors within the detector channel, i.e., the real-time processor receives 32 bins in total. After determining the lateral position of the particle from the summed data of both detectors, the value was transferred back to the FPGA for the next rotation period provided the binned signal exceeds a user-defined threshold (typically 5 kHz). When the signal falls below the given threshold, the particle was considered to be outside of the orbit and a search algorithm is started. In parallel, the data were streamed to the host computer (non-deterministic unit) via a gigabit Ethernet connection and written to a solid-state disc as a text (.txt) file. The text file

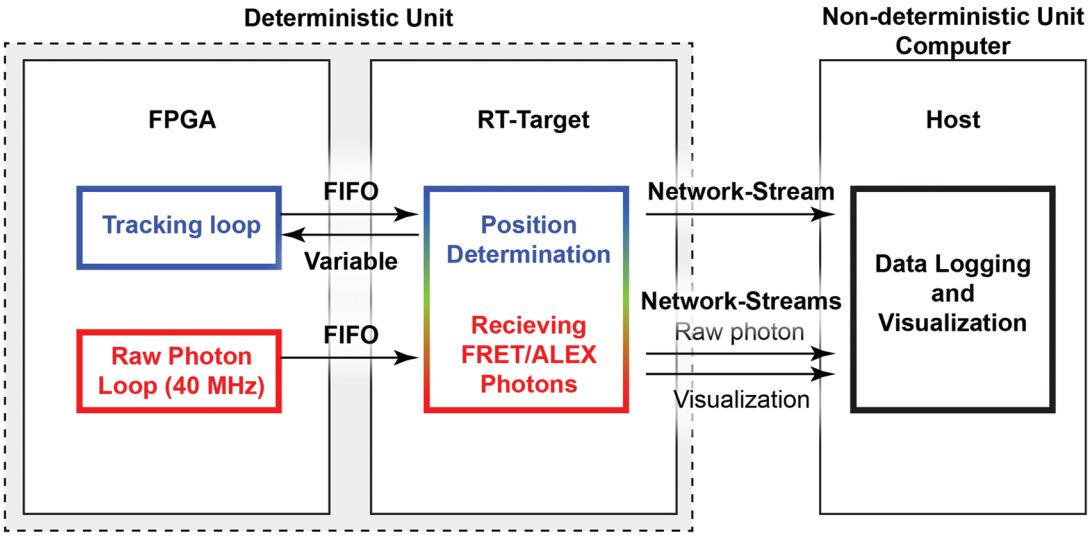

Figure 1. Flow chart of data acquisition for the Tracking/spFRET modality.

contains the 3D position information and intensities for each channel.[26] In addition to receiving the data, the host computer generally controls the real-time unit, i.e., it defines experimental settings, starts and stops the tracking algorithm, and visualizes the received tracking data during the experiment.

The above-described procedure summarizes the overall software architecture for one tracking channel. For dual-color experiments, both tracking channels were read-out independently. One .txt file was generated per each tracking channel, in which the data per detector-pair were written. Here, the real-time unit alternates the data acquisition and streaming to the real-time processor for each tracking channel resulting in a decrease of time resolution by a factor of 2–10 ms for the experiments here. The software discriminates between the three tracking modalities described in this publication as follows:

1) For independent dual-color, real-time tracking experiments, the unit treats each tracking channel independently. The real-time processor calculates the position of each particle and transfers the information to the FPGA, i.e., the instrument switches between both particle positions alternatingly. When the fluorescence intensity of a particle in one channel falls below the tracking threshold, the search algorithm is executed in the corresponding channel while the second particle is still tracked.
2) When probing correlative motion, one tracking channel is defined as the "leading channel". After orbiting around the particle in the leading channel, the data are streamed to the real-time processor for position calculation and the feedback algorithm applied. The next orbit is performed at the updated position with the excitation laser of the second channel. The data from the second orbit are transferred to the real-time unit, which directly streams it to the host without a position update. Now, the next orbit is executed for the "leading channel". In this mode, the search algorithm is only started when the detected count-rate is below the threshold of the leading channel.
3) In the tracking/FRET modality, one tracking channel is set as the leading channel for position determination while the other channel monitors the fluorescence signal of the tracked FRET pair. The data acquisition, streaming, and position update are the same as described above in the case of correlative motion. After performing an orbit for the tracking channel, a spatially identical orbit is performed for either direct donor or acceptor excitation according to the ALEX sequence. One complete cycle comprises: tracking channel, acceptor excitation, tracking channel, donor excitation.

The TTL signal of each detector was acquired with the 40 MHz time resolution given by the onboard clock of the FPGA. In addition to the micro-time, which was given as the number of clock cycles since the last photon was detected, each detected photon was tagged with further information regarding the orbit number, orbit segment, detector number, and excitation laser. All information was multiplexed into a 64-bit unsigned integer and transferred in separate data FIFO1 to the real-time processor (Figure 1). To have a live update of the FRET signal on the host computer, the detected photons during donor and acceptor excitation are also binned in user-defined time intervals and the values were transferred using a FIFO2 and network stream (visualization stream, Figure 1). This data transfer was executed independently from the tracking algorithm on the FPGA. On the host, the received data from the FRET stream was written into a binary sidecar file consisting of the same name as the .txt file. The binned count-rate received from the visualization stream was monitored to inform the user about the presence of the FRET pair.

2.3.3. Tracking Algorithm

The implemented 3D tracking algorithm separates the position determination for the lateral and axial localization. The total intensity from both detectors was used to calculate the lateral position. This signal was measured along the orbit and binned into 16 different positions and expressed as a Fourier series with coefficients up to the 16th order ($k = 16$):

$$I(\varphi, r) = \frac{a_0(r)}{2} + \sum_{k=1}^{16} \left(a_k(r)\cos(k\varphi) + b_k(r)\sin(k\varphi)\right) \tag{1}$$

The lateral position of the particle with respect to the center of the orbit is encoded in the zero- and first-order coefficients obtained from a Fast Fourier Transformation. The angular position, φ, and the radial distance, d_r', from the orbit center can be calculated from the zero- and first-order coefficients as follows:

$$\begin{aligned} \varphi &= \tan^{-1}\left(\frac{b_1}{a_1}\right) \\ d_r' &= r_{\text{orbit}} \cdot f(r) \cdot \frac{\sqrt{a_1^2(r) + b_1^2(r)}}{a_0(r)} \end{aligned} \tag{2}$$

where r_{orbit} is the radius of the orbit and $f(r)$ is a theoretically determined scaling function that converts the modulation of the signal to a distance. The axial localization is accessible by comparing the difference in signal between one detector pair. The particle position d_z' with respect to the focal plane can be calculated as follows

$$d_z' = \Delta z \cdot g(z) \cdot \frac{I_{APD1} - I_{APD2}}{I_{APD1} + I_{APD2}} \tag{3}$$

where Δz is the distance between the detection planes of APD1 and APD2, which are positioned equidistantly above and below the actual focal plane, and $g(z)$ is the corresponding scaling function for z. Both scaling functions are implemented as lookup tables to decrease the computation time. Slight differences in the effective detection efficiency for the two detectors in a detection pair will lead to an offset in the position of the particle from the actual focal plane. However, this z-offset does not impact the determined trajectory and the z-feedback loop aims to equalize the counts between the two APDs. For two color tracking, the offset from the focal plane along with chromatic aberrations leads to an offset between the two tracking channels. As the objective is moved in the z-dimension using a piezo stage for the axial tracking routine, this offset is independent of the absolute z-position and is found to vary only slightly in the x-y plane (Figure S1, Supporting Information).

2.3.4. Data Collection and Analysis

As described above, dual-color tracking experiments can be carried out in two different ways: 1) both tracking channels are treated independently, or 2) the software actively tracks the movement of one particle and probes its surrounding for the second particle. In both variations, the corresponding laser lines can either be simultaneously activated or alternated.

Image Calibration and Dual Color Localization Experiments: When measuring the position of multifluorescent beads that were detectable in both detection channels, it was evident that this microscope had a significant shift between the two channels. The main contribution of this offset originates from the chromatic aberrations of the telescope optics between the galvanometer mirrors and the objective, which were crucial for good scanning and imaging. Hence, it was necessary to register the two detection channels to correct for the aberrations. The chromatic aberrations could also be minimized by purchasing optimized lenses, as it was shown recently for another microscope system.[27]

To register the positions of the two detection channels, a transition matrix was determined using multifluorescent beads. One hundred microliters of the stock solution (0.2%) of multifluorescent beads was diluted 100-fold in PBS, added to an untreated LabTek chamber and allowed to sediment for 10 min. The beads were then tracked for 5,000–10,000 orbits. The red detection channel was defined as the leading channel for actively tracking one particle and the blue detection channel as the passive localization channel for determining the position from the second signal. Using the position reconstruction from the fluorescent signal of the blue channel, the coordinates were mapped onto the leading channel generating a transformation matrix. The geometric transformation function *fitgeotrans* from MATLAB was used to calculate the transformation matrix. The experiment was repeated with Atto488 labeled, red-emitting avidin coated beads. One hundred microliters of a 100-fold diluted 0.1% suspension was mixed with 100 µL of a 100 pM Atto488-biotin solution and incubated for 10 min. The mixture was then added to an untreated LabTek chamber. The beads were tracked with the same settings for 5,000 orbits each after 10 min of sedimentation time. Whenever the spectral range of one of the tracking channels is changed, the transformation matrix needs to be redetermined.

Dual-Color 3D Orbital Tracking Experiments: Dual-color tracking experiments were demonstrated by using 488 and 633 nm excitation to update the position of a particle in the leading channel first and consecutively localize the second particle (independent motion) or its emission (correlative motion). All experiments were carried out at laser powers of 0.32 µW for 488 nm and 0.42 µW for 633 nm laser excitation measured before the microscopy body. The orbit-time for each channel was set to 5 ms.

For independent dual-color tracking, two 0.1% particles suspensions of ≈500 nm size beads were mixed (see Section 2.1, Materials and Chemical section for further details). Two microliters of the "yellow" beads and 10 µL of "purple" beads were mixed with 188 µL PBS and directly added to the passivated LabTek chamber for the measurements.

For correlative dual-color tracking, a 100-fold diluted suspension of 0.1% "purple" particles was labeled with biotinylated Atto488. Here, 100 µL of the pre-diluted particle solution was added to 100 µL of a 100 pM Atto488-biotin solution and incubated for 10 min. As the vast majority of the fluorophore is bound to the avidin-coated beads, no purification step was necessary afterwards. The sample was then directly diluted with buffer to a final volume of 750 µL containing 1% (w/v) Glucose, 10% (v/v) Glycerol, 1 mM Trolox, and 10% (v/v) Glucose-Oxidase/Catalase system for photo-stabilizing the Atto488. This imaging mix was immediately added to a passivated chamber of an 8-well LabTek slide and sealed. Experiments were started after waiting for an additional 5 min for oxygen removal.

Tracking/spFRET Experiments: For 3D FRET-tracking, the microscope alternates between reading out the position in the tracking channel 1 (488 nm excitation) and probing the FRET signature of the sample in the second channel. ALEX excitation was used at 633 and 561 nm with position determination, probed at 488 nm. For slowly diffusing objects, the donor and acceptor excitation times can be performed for an integer number of orbits before switching to 488 nm excitation for updating the position of the particle. 3D FRET/tracking measurements were carried out using 12 µW for 488 nm, 88 µW for 561 nm, and 18 µW for 633 nm excitation measured before the microscope body.

To extract the distance of fluorescent labels on diffusing dsDNA via FRET, the dsDNA oligos were attached to slowly diffusing streptavidin-coated silica beads (#CS01000-2; Polysciences Europe GmbH). For this, 1 µL of the 146 pM bead suspension was added to 50 µL of 5 pM dsDNA and pre-incubated the mixture for 5 min. During mixing, a few beads were bound with a high concentration of dsDNA but the majority of beads ended up with either one or no dsDNAs attached. Afterwards, 50 µL of 60 pM Atto488-biotin was added to the mixture and allowed to incubate for 5 min. For photostabilization, the prepared solution of 101 µL was filled to a total volume of 750 µL of PBS containing 1% (w/v) glucose, 10% (v/v) glycerol, 1 mM Trolox, and 10% (v/v) mixture of the glucose-oxidase/catalase system (6.25 µM glucose-oxidase in 40% glycerol and 2 mM TCEP; 400–800 nM catalase). This imaging mix was immediately added to a passivated chamber of an 8-well LabTek slide and sealed. First measurements were started after allowing 5 min for oxygen removal.

Data Analysis: The obtained data from dual-color tracking experiments were loaded and analyzed with home-written scripts in MATLAB2018a. The FRET data collected during tracking were analyzed with a home-written program developed in LabVIEW2018. After loading the tracking and sidecar files, the full data were extracted and converted into time bins of 50 ms. Next to the information from the first tracking channel including intensity and its 3D trajectory, the software extracts the donor as well as acceptor intensities and calculates the FRET efficiency for the second detection channel. Next, the extracted traces were manually inspected for active tracking in the tracking channel. Otherwise, the respective data files were excluded from further analysis.

1) Diffusion analysis

Theoretical diffusion coefficients of beads were calculated using the Stokes–Einstein Equation

$$D = \frac{k_B T}{6\pi\eta r} \tag{4}$$

where k_B is the Boltzmann constant, T the temperature, η the viscosity of the buffer, and r the hydrodynamic radius of the particle.

Diffusion coefficients for the measured traces were determined using the mean squared displacement (MSD) approach

$$MSD(t) = \left\langle \left(\vec{r}(t+t') - \vec{r}(t')\right)^2_{t'} \right\rangle \tag{5}$$

where $\vec{r}(t)$ is the 3D trajectory of the particle. For reliable results, the MSD was calculated over a quarter or an eighth of the trajectory data, depending on the length of the trace. MSD plots of traces showing Brownian motion (correlative tracks) were fitted to

$$MSD(t) = 6Dt \tag{6}$$

with t representing the lag time between data points and D the diffusion coefficient. MSD plots of traces exhibiting diffusion with a flow were fit using:

$$MSD(t) = 6Dt + (Vt)^2 \tag{7}$$

where V is the flow velocity of the medium.

For motion in cells, one typically observes multiple types of diffusional behavior. To summarize directed transport, Brownian diffusion and anomalous diffusion, the MSD plots were fitted to a generic equation:

$$MSD(t) = b\,t^{\alpha_D} \tag{8}$$

where the exponent, α_D, indicates the type of motion and b is related to the respective diffusion or velocity.[28] For α_D, the MSD was interpreted as directed transport with $b = V^2$. For $\alpha_D \sim 1$ and $\alpha_D < 1$, the motion in these regions of the trajectory was interpreted as normal diffusion or anomalous diffusion, respectively, with $b = 6D$.

2) SpFRET analysis

All trajectories were inspected and characterized as FRET traces when they exhibited either single-step photobleaching of the FRET pair or count rates compatible with single fluorophores. Regions within the selected traces were then categorized as: 1) FRET signal, 2a) donor only or 2b) acceptor only, and 3) as background. Bead specific background correction was performed when possible.

$$bg_{XY} = \frac{1}{\left(n_{\text{stop}} - n_{\text{start}} + 1\right)} \sum_{\text{start}}^{\text{stop}} B_{XY}(t) \tag{9}$$

where B_{XY} is signal intensity of the background measured with X laser excitation and Y detected emission channel for the particular bead, and n represents starting and stopping data points for the selected region. Otherwise, tracked beads not exhibiting a DNA label were used to categorize the background due to scattering or impurities in the buffer. The average background values from non-labeled beads were calculated for each channel ($\overline{B}_{XY}$). The calculated background was then subtracted from the measured fluorescence signal

$$F_{C,XY}(t) = F_{XY}(t) - bg_{XY} \tag{10a}$$

or

$$F_{C,XY}(t) = F_{XY}(t) - \overline{B}_{XY} \tag{10b}$$

After categorizing the corresponding intensity traces and applying background correction for each tracked particle, the correction factors for direct excitation α, spectral cross talk β, and detection sensitivity γ were determined.[25,29] The molecule-wise correction factor α for direct excitation was derived from "acceptor only" traces according to

$$\alpha = \frac{1}{\left(n_{\text{stop}} - n_{\text{start}} + 1\right)} \sum_{t_{\text{start}}}^{t_{\text{stop}}} \frac{F_{DA}(t)}{F_{AA}(t)} \tag{11}$$

Similarly, the correction factor β for spectral cross talk was derived from "donor only" traces, by taking the ratio of:

$$\beta = \frac{1}{\left(n_{\text{stop}} - n_{\text{start}} + 1\right)} \sum_{t_{\text{start}}}^{t_{\text{stop}}} \frac{F_{DD}(t)}{F_{DA}(t)} \tag{12}$$

In traces exhibiting acceptor photobleaching, the correction factor γ was derived by

$$\gamma = \frac{\left(\frac{1}{\left(n_{1,\text{stop}} - n_{1,\text{start}} + 1\right)} \sum_{t_{1,\text{start}}}^{t_{1,\text{stop}}} F_{DA}(t)\right) - \left(\frac{1}{\left(n_{2,\text{stop}} - n_{2,\text{start}} + 1\right)} \sum_{t_{2,\text{start}}}^{t_{2,\text{stop}}} F_{DA}(t)\right)}{\left(\frac{1}{\left(n_{2,\text{stop}} - n_{2,\text{start}} + 1\right)} \sum_{t_{2,\text{start}}}^{t_{2,\text{stop}}} F_{DD}(t)\right) - \left(\frac{1}{\left(n_{1,\text{stop}} - n_{1,\text{start}} + 1\right)} \sum_{t_{1,\text{start}}}^{t_{1,\text{stop}}} F_{DD}(t)\right)} \tag{13}$$

where regions 1 and 2 are regions of the trace selected before and after acceptor photobleaching, respectively. For cases where bead-specific correction factors could not be calculated, the average value was used instead (i.e., $\overline{\alpha}$ for direct excitation, $\overline{\beta}$ for spectral cross talk, and $\overline{\gamma}$ for detection efficiency). Using the determined correction factors, a corrected FRET efficiency value E was calculated:

$$E(t) = \frac{F_{DA}(t) - \overline{\alpha} F_{AA}(t) - \overline{\beta} F_{DD}(t)}{F_{DA}(t) - \overline{\alpha} F_{AA}(t) - \overline{\beta} F_{DD}(t) + \overline{\gamma} F_{DD}(t)} \tag{14}$$

A particle-wise averaged FRET efficiency was then calculated. The FRET efficiency and uncertainty of the different FRET constructs were given by the peak and standard deviation of a Gaussian fit to the spFRET histogram.

2.4. SpFRET PIE-MFD Experiments

Solution-based, spFRET experiments on dsDNA were performed on an inverted, confocal microscope (Ecclipse Ti, Nikon, Germany) equipped with 565 nm (LDH-D-TA-560, PicoQuant, Germany), and 640 nm excitation (DH-D-C-640, PicoQuant, Germany). The average excitation intensities for dual color measurements were 80 µW at 565 nm and 30 µW at 640 nm. The resulting fluorescence was separated from the excitation beams via a polychroic mirror (zt405/488/561/633, AHF; Germany), passed through a confocal pinhole (75 µm) and separated via polarization using a polarizing beamsplitter (PBS251, Thorlabs, Germany). The fluorescence was then split

spectrally via additional dichroic mirrors (BS560 and 640DCXR, AHF; Germany) and cleaned up with the appropriate emission filters (ET525/50 for the blue channel; ET607/36, AHF, Germany for yellow detection; ET670/30, AHF, Germany for red detection). Photons were detected using photon-counting APDs (Count-100B, Laser Components, Germany; 2x SPCM AQR-14/2x SPCM AQR-16, PerkinElmer, USA) and registered by independent but synchronized time-correlated single-photon counting (TCSPC) hardware (HydraHarp400, PicoQuant, Germany). The detector signal was recorded using a home-written program in C#.

The recorded data were evaluated using *PAM*[30] to characterize the double-labeled dsDNA constructs. The FRET efficiency, labeling stoichiometry, fluorescence lifetime and anisotropy were determined. To calculate these various parameters, the detected fluorescence photons were sorted according to the detection channels (donor detection channel: D; acceptor detection channel: A) and excitation source, which is encoded in the photon arrival time. Burst selection was performed by considering detected photons to belong to a single burst as long as the local count rate within a sliding window exceeded a certain threshold (5 photons within 500 µs or 10 kHz for the experiments performed here). Only bursts with a minimum of 50 photons were further analyzed. After burst selection, the bursts were additionally filtered using a minimum of at least 150 photons and an ALEX-2CDE filter[31] between 0 and 30. After background subtraction, the uncorrected proximity ratio E^* and labeling stoichiometry S^{raw} were calculated for each fluorescent burst characterized by three photon-streams, i.e., by its donor-based donor emission F_{DD}, donor-based acceptor emission F_{DA} and acceptor-based acceptor emission F_{AA}.

$$E^* = \frac{F_{DA}}{F_{DD} + FF_{DA}} \tag{15}$$

$$S^{raw} = \frac{F_{DD} + F_{DA}}{F_{DD} + F_{DA} + F_{AA}} \tag{16}$$

While E^* monitors the proximity between both fluorophores, S^{raw} describes the ratio of donor-to-acceptor intensities. After binning the detected bursts into a 2-D E^*-S^{raw} histogram,[25,29] the contribution of direct excitation $\alpha' = S^{raw}_{AO}/(1 - S^{raw}_{AO})$ is derived by the acceptor-only population (AO). Using the uncorrected proximity ratio E^*_{DO} of the donor-only population (DO) allows for determining the amount of spectral cross talk $\beta' = E^*_{DO}/(1\text{-}E^*_{DO})$ into the acceptor channel. After correction of spectral cross talk, direct excitation, as well as differences in detection sensitivities between the channels,[25] the corrected FRET efficiency E and stoichiometry S are given by

$$E = \frac{F_{DA} - \alpha' F_{AA} - \beta' F_{DD}}{F_{DA} - \alpha' F_{AA} - \beta' F_{DD} + \gamma F_{DD}} \tag{17}$$

$$S = \frac{F_{DA} - \alpha' F_{AA} - \beta' F_{DD} + \gamma F_{DD}}{F_{DA} - \alpha' F_{AA} - \beta' F_{DD} + \gamma F_{DD} + F_{AA}} \tag{18}$$

The fully corrected FRET efficiency is related to the distance between donor and acceptor r using:

$$E = \frac{1}{1 + \left(\frac{r}{R_0}\right)^6} \tag{19}$$

where R_0 refers to the Förster radius, i.e., the distance between donor and acceptor fluorophores at which the FRET efficiency is 50%. The Förster radius for fluorophore pairs in this study (Atto565-Atto647N) was taken to be 69 Å.

3. Results

The multicolor 3D orbital-tracking setup developed in this work was implemented based on a previously described confocal microscope.[12] A schematic representation of the orbital tracking approach is given in **Figure 2**A. By circularly rotating the laser excitation volume of the confocal microscope around the diffusing particle, the fluorescence signal will be modulated differently depending on its position within the orbit. By performing a fast Fourier transformation (FFT) on this signal, the phase and amplitude modulation of the emitted fluorescence can be determined, which encode the particle position with respect to the orbit center and allow for lateral tracking. To obtain axial information at the same time, we implemented a detector pair. The detected signal is split equally between both APDs via a beam-splitter (Figure 2B) and the detection volumes of both APDs are equidistantly positioned out-of-focus. They are positioned above and below the focal planes via two separate lens systems and multimode fibers are used as confocal pinholes for defining the detection volume. The signal from both detectors is added together for lateral tracking while the intensity ratio is used for axial tracking (see Experimental Section). With the 3D information at hand, a feedback loop is used to re-center the orbit of the microscope on the diffusing particle and enables single-color, real-time 3D orbital tracking.

To enable dual-color 3D orbital tracking and/or reading-out of the spectroscopic signatures of a tracked particle, the instrument is equipped with two pairs of detectors and three laser lines at 488, 561, and 633 nm (Figure 2B). For generating the orbit of the laser beam, galvanometric mirrors are used. The system is also equipped with a wide-field modality to visualize the environment around the particle being tracked. Diffusing particles in the sample were tracked using orbit repetition rates of up to 200 Hz. After excitation, the resulting emission of the sample was detected on the two pairs of APDs. Using this configuration, experiments with three different modalities can be performed: 1) the dual-channel tracking configuration in which both channels alternatingly measure the position of two independent particles (Figure 2C), 2) correlative motion where we actively track the particle in three dimensions in one channel while alternatively determining the position of the second fluorescent species in the second channel (Figure 2D), or 3) the tracking of channel 2 was modified for reading out the spFRET signature of the tracked molecule (Figure 2E).

3.1. Independent Dual-Color Tracking

Dual-color tracking experiments were carried out in two different configurations. We first targeted the independent motion

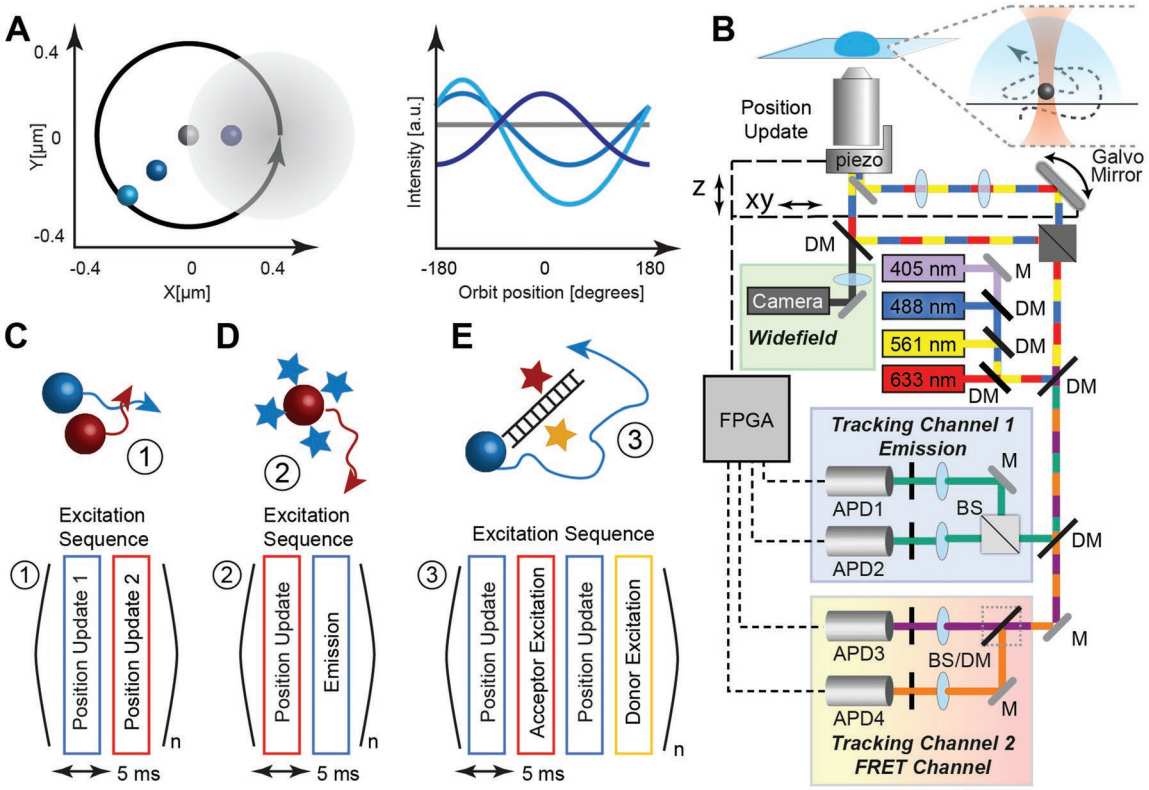

Figure 2. Dual-color, real-time 3D Orbital-Tracking: setup, theory, and excitation sequences for the implemented modalities. A) The principle of orbital tracking: left, the laser (grey shaded area) is rotated in an orbit (black circle) generating a fluorescence signal depending on the position of the emitters (depicted as grey and blue spheres) with respect to the orbit. Right, a schematic of the modulated signal is shown for the corresponding positions shown in the left panel. B) Schematic of the instrument. Three excitation lasers are guided onto a galvanometer-driven, two-axis mirror system for generating the orbit. A 60x water objective focuses the beam into the specimen. The fluorescence signal is collected by the same objective and relayed to the detection pathway by a PM. The signal is spectrally separated between the two detection channels via a DM. In each detection channel, the light is either split into two focal planes or into additional spectral regions, and focused on multimode fibers, which act effectively as confocal pinholes and guide the light to the APDs for detection. The detectors are connected to a FPGA which repositions the laser beam via an active feedback loop. Abbreviations: APD, avalanche photondiode; BS, beam splitter; FPGA, field-programmable gate array; PM, polychroic mirror; DM, dichroic mirror; M, mirror; PH, multimode fiber acting as a pinhole. C–E) Multi-color 3D orbital tracking modalities. Spectrally different particles can be tracked C) independently, D) correlatively or E) with spectroscopic readout. The corresponding excitation sequences for the implemented modalities are depicted below. Each rectangle represents one full orbit of the corresponding laser wavelengths. For the worked presented here, an orbit-time of 5 ms was used.

of two different emitters by alternatingly tracking their position in two separated detection channels. This is similar to the multiplexing approach that allows multiple particles to be tracked simultaneously using orbital tracking[32] but with different spectral signatures. To benchmark our instrument and approach, we first checked how accurately we could localize stationary, multifluorescent beads on a coverslip (**Figure 3**A). A clear shift between detection channels is observed. This is to be expected because chromatic corrections over the large excitation and detection range (488–700 nm) need to be applied. However, even with a well chromatically corrected systems, a registration of the two channels will be necessary to optimize the precision of the data on the nm scale. After applying the transformation matrix (Figure 3A, right panel, see Experimental Section for details), we could localize the beads in both channels with an accuracy of <5 nm and a precision of <15 nm (Figure 3B) in the *x*-*y* plane. We concentrate here on the axial mapping, as it is significantly influenced by chromatic aberrations. The axial dimension has a chromatic shift of 47 nm, which is fairly independent of the lateral position (Figure S1, Supporting Information). For the calibration experiments, typical count rates for the individual beads were between 15 and 90 kHz in the blue channel, and between 35 and 400 kHz in the red channel.

In the next step, we mixed two kinds of fluorescent polystyrene beads and tracked them in solution. One kind of bead is 450 nm in size and emits between ≈460 and 540 nm (measured with 488 nm excitation; blue detection channel). The second kind of bead is 560 nm in size and emits between 580 and 650 nm (measured with 561 nm excitation; red detection channel). Representative data from two independently diffusing particles are shown in **Figure 4**A (blue trace). Further examples are provided in Figure S2 (Supporting Information). The blue particle was constantly tracked over ≈5.0 s with a sensitivity threshold of 5 kHz for position detection (Figure 4A). This threshold defines whether a particle is within the orbit or if the instrument switches to the search algorithm. The measured 3D trajectory is shown in Figure 4B, where the temporal information is color-coded in the trace changing from blue-to-green.

Similarly, the red fluorescence (Figure 4A; red trace) was used to track the 3D position of the second particle. Its

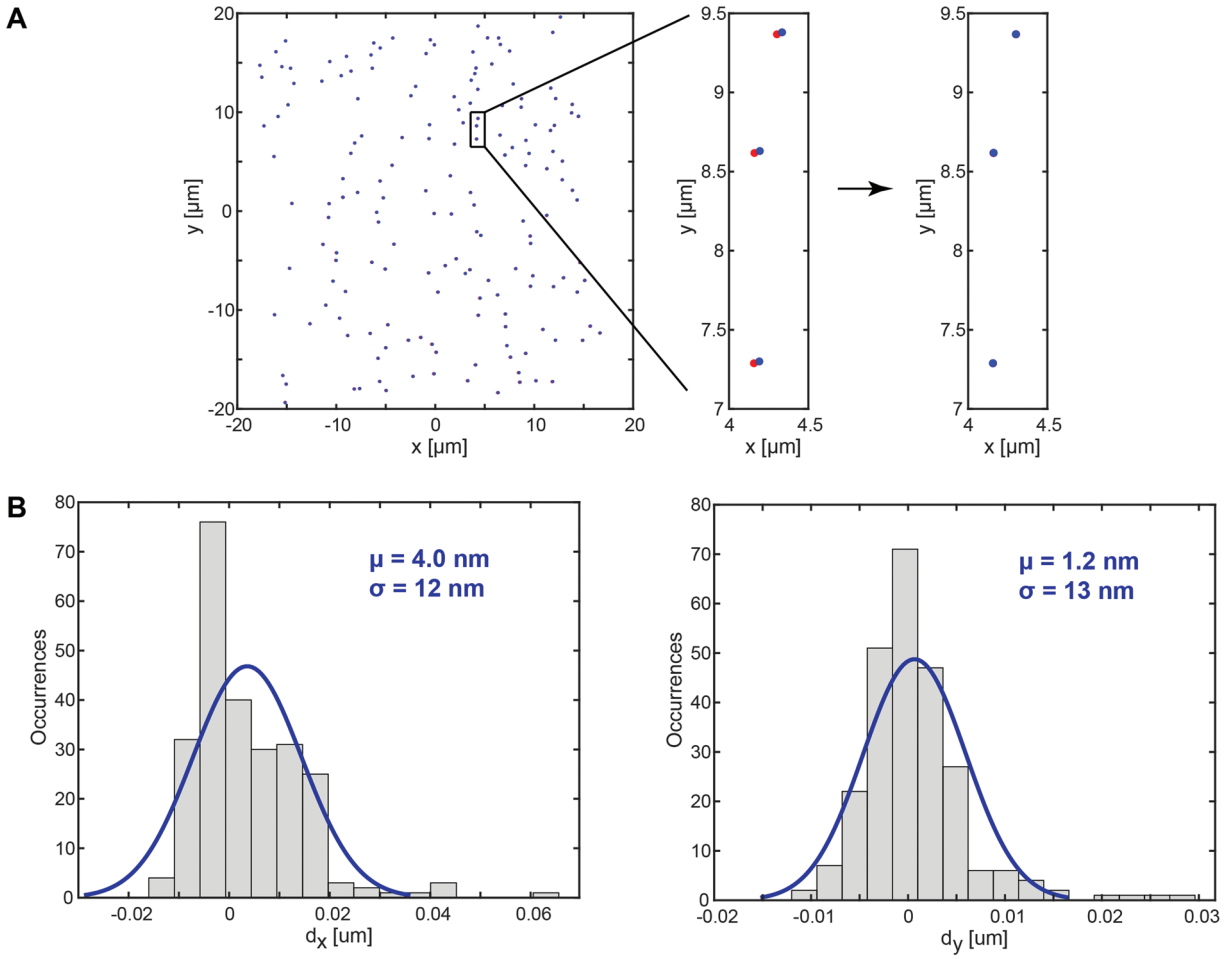

Figure 3. Image calibration and corrected registration of the two channels. A) Tracked positions of calibration beads covering the field of view. Red and blue circles represent the center of mass coordinates for the respective channel. The offset between the channels originating from chromatic aberrations is shown in the middle panel. After performing the mapping procedure, the blue detection channel is corrected. B) Histograms of the measured distance between the blue and red signal from individual beads along the x- and y-axis are shown for red-fluorescent beads labeled with Atto488 after applying the image transformation.

corresponding trajectory in solution is shown in Figure 4B. The spirally shaped motions at roughly 3.25 and 3.75 s (shown in light grey) indicate activation of the search algorithm as the corresponding bead was lost by the microscope for a short period of time. This happens when the detected emission falls below the set sensitivity threshold, which occurs more frequently with the red beads due to their approximately fourfold lower intensity. The distance between both particles (Figure 4C) varies during the observation time by >20 µm. Due to the relatively fast motions of the freely diffusing beads, we only collect one orbit at the previously determined location when alternating between beads. This leads to the large fluctuations observed in Figure 4A. If the objects were moving more slowly or if faster opto-mechanics were utilized in the system, one could perform a few orbits to lock in accurately on the particle, which would decrease the intensity fluctuations. However, as the position of the particle is determined via the phase and modulation of the signal, the absolute intensity does not have a dramatic influence on the location accuracy.

An analysis of the relative movement of both beads clearly indicates that their motions are independent. This can also be seen by comparing the relative and absolute mean-square-displacement (MSD) plots (Figure S3A, Supporting Information). For independent motion, the relative distance has a higher diffusion coefficient than the absolute displacement of either bead. In addition, the MSD (Figure S3A, Supporting Information) also reveals that their diffusion is not dominated by Brownian motion but by turbulence induced upon the addition of the nanoparticles to the imaging buffer. Diffusion with flow is also observed for other example trajectories shown in Figure S2 (Supporting Information). We verified that the turbulence is not introduced by the z-oscillations of the objective switching between particles by performing an MSD analysis on the xy-projected trajectories. Flow is still observable in planes orthogonal to the motion of the piezo. The 3D MSD analysis returned the same average flow rate of 1.7 µm s^{-1} for both particles but was found to decrease over the course of the trajectory. The blue particle has a diffusion coefficient of 0.84 ± 0.04 µm^2 s^{-1}, while the red bead diffuses slightly faster with a diffusion coefficient of 1.03 ± 0.05 µm^2 s^{-1}. Using

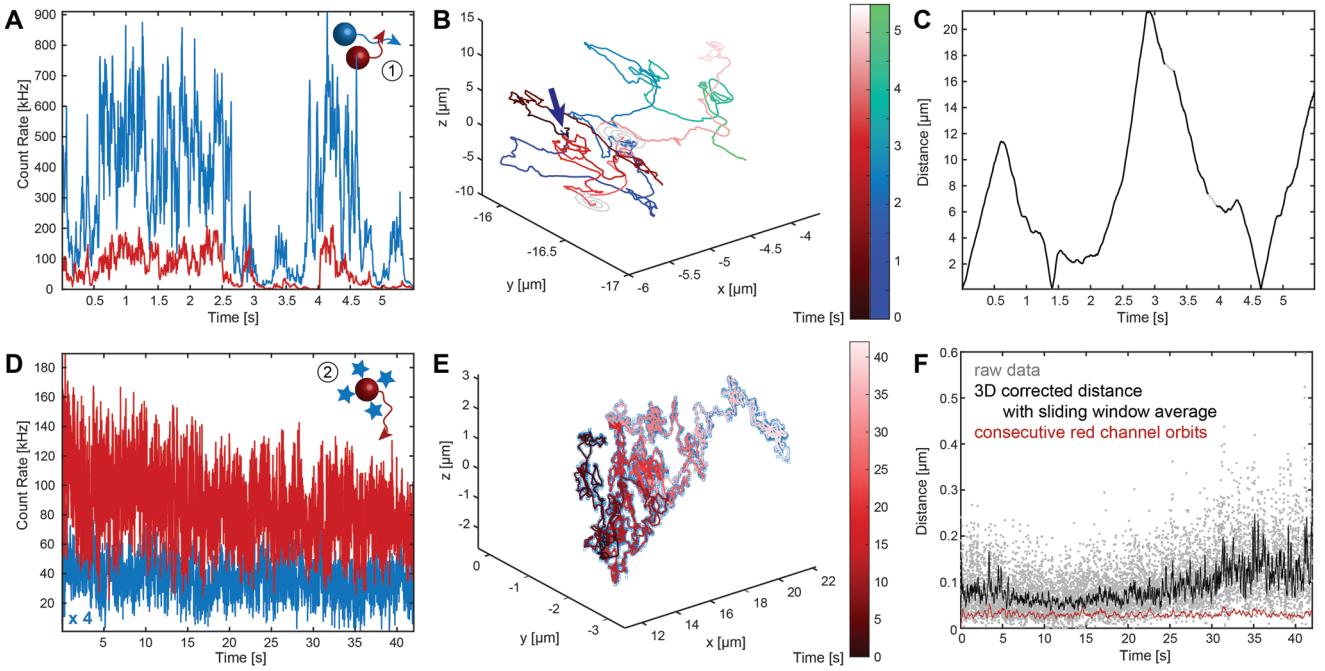

Figure 4. Dual-Color Tracking of beads. A–C) Independent motion: A) fluorescence intensities, B) 3D trajectories, and C) relative distance between the two independently diffusing particles. The beginning of the trajectories is indicated by the arrow in panel (B). The particles exhibit separations of up to 20 µm. The blue intensity and blue-to-green color-coded trace correspond to the particle excited at 488 nm. The red signal and the black-to-red color-coded track correspond to the bead excited at 633 nm. The grey data points in panels B and C indicate regions when the red particle was not detected within the orbit. D–F) Correlative motion: D) fluorescence intensities of the red and blue signals corresponding to the fluorescent emission of the bead (with 633 nm excitation) and dye (with 488 nm excitation). To make it more visible, a factor of four has been applied to the intensity of the blue channel. E) A 3D correlated trajectory of a red-emitting bead labeled with Atto488. The red trace represents the position of the red particle and the blue cloud surrounding the trace depicts the localization of Atto488 probed during tracking of the red particle. F) The distance between emission from the red particle and the Atto488 signal (grey). The solid lines represent a sliding window average of 50 orbits for the correlative tracking (black) and for consecutive orbits of the tracking channel (i.e., the red channel in this case shown in red).

the Stokes–Einstein relation, a fixed temperature of 20 °C and the viscosity for pure PBS medium[33] at 20 °C of $\eta = 1.0192$ mPa-s, the hydrodynamical radius r of each particle can be estimated. For the blue particle, we found a radius of ≈350 nm (or 700 nm diameter), and a radius of ≈370 nm (740 nm diameter) for the red bead. Both values are larger than the average value radius provided by the supplier (Experimental Section) of 225 and 280 nm, respectively. We also measured the size distribution of the beads using scanning electron microscopy (SEM). The dried beads have a size distribution centered ≈200 nm radius (or 400 nm diameter, Figure S4, Supporting Information) with the blue beads having a slightly larger radius. The hydrodynamic radius determined from orbital tracking deviates from what is expected from the measured particle sizes. However, the absolute values are difficult to compare due to the distribution in bead sizes, protein coating and solvation shell, and uncertainty in the exact solvent composition. We consistently observe a slower diffusion coefficient on average for the larger beads and have the advantage of measuring the diffusion coefficient directly on the tracked bead of interest under the exact experimental conditions.

3.2. Correlative Dual-Color Tracking

Often, it is sufficient to measure the distances between two particles when they are interacting, in which case, a correlative dual-color tracking approach can be used. To implement 3D orbital-tracking of two emitters that show correlative motion, one channel is defined as the leading channel and used for actively tracking one of the particles where the second channel is used to passively localize the second particle. This provides higher localization accuracy with the same time-resolution when the two particles are within the laser orbit radius. Figure 4D,E depicts the intensity (left panel) and 3D trajectory (right panel) of streptavidin-covered red-emitting beads that are coated with biotinylated Atto488 (further examples are given in Figure S5, Supporting Information). The gradient-coded trace (Figure 4E) represents the Brownian motion of the dual-labeled bead. The blue clouds represent the detected emission of the attached Atto488 probed by alternating laser excitation. To verify that scattering is not the origin of this measured signal, control experiments were performed in the absence of Atto488 (Figure S6, Supporting Information) where no signal was detected in the blue channel. As expected for dual-color particles, the distance between both emitters did not change during the tracking experiment (Figure 4F). The relative separation between the particles was found to be $\lesssim$100 nm, which is explained by the temporal delay of 5 ms between the alternating orbits. The quasi-identical trajectories share a common diffusion coefficient D of 0.11 µm^2 s^{-1} derived from the MSD analysis (Figure S3B, Supporting Information). The derived hydrodynamic radius $r = 980$ nm of the Atto488-labeled particle

is significantly larger than the reported radius (290 nm) for the unlabeled red bead, which suggests we were tracking an aggregate in this case.

We observed that the achieved tracking duration for two independent particles is generally shorter than for single-particle tracks as well as dual-color trajectory measured in correlative mode since the instrument has to continually jump between the two particle locations between each orbit. The main limiting factor here is the response time of the z-Piezo nanopositioner for the objective. Hence, the axial position of the particle may not be perfectly matched, leading to a faster loss of the particle. This could be circumvented by decreasing the alternation frequency between the particles. However, this has to be balanced with the motional speed of the particle such that, upon returning to the previously known location, the diffusing particle has a high probability of still being within the orbit.

For tracking correlative motion, the offset between both channels is mainly biased by two phenomena, diffusion and chromatic aberrations originating from the telescope system. Due to the delay between orbits with different excitation wavelengths, there is a shift in the position of the particle. This could be eliminated by combining orbital tracking with pulsed interleaved excitation.[34] Chromatic aberrations of the telescope system can also be corrected for to some extent via calibration and applying a mapping algorithm. In this case, specially designed telescope lens can be implemented to dramatically improve the overlap between the two channels as we have recently demonstrated on a laser scanning confocal microscope setup.[27]

3.3. Spectroscopic Readout during 3D Orbital Tracking

Next, we expanded our dual-color 3D orbital tracking approach to allow spectroscopic investigations in the second channel. In particular, we performed single-pair FRET measurements on diffusing particles. Here, we replaced the 50/50 beamsplitter used above with a dichroic mirror in the second channel such that we can measure single-molecule FRET while tracking the sample in the first channel (Figure 2B). For these experiments, double-labeled, double-stranded DNA (dsDNA) was linked to the surface of streptavidin-coated silica beads (0.48 µm diameter), which were labeled with Atto488-biotin (at a ratio of 1:20). To minimize multiple DNA strands being bound to the same particle, an oligonucleotide concentration of 5 pM was used during incubation with the labeled bead. The Atto488 fluorescence was used for tracking while spFRET was measured between the FRET pair Atto565 and Atto647N attached to the dsDNA.

3.3.1. Sample Characterization by MFD-PIE

Before performing the orbital tracking experiments, we characterized the dsDNA samples in solution using multiparameter fluorescence detection[35] with pulsed interleaved excitation[34] (MFD-PIE; see Experimental Section).[25] Three dsDNA strands labeled at different positions were used to generate a low, intermediate, and a high FRET signal (**Figure 5**A and Scheme 1). The top strand was labeled with an acceptor fluorophore Atto647N (at position 27) and was biotinylated at the 3′-end for immobilization on the silica beads. The bottom strand carries the donor fluorophore Atto565 at either position 6 (DNA1), position 12 (DNA2) or position 18 (DNA3). The accessible positions of the attached dyes along the DNA were determined using AV simulations[36] (Figure S7, Supporting Information) and are depicted as red or green clouds along the DNA helix in Figure 5A.

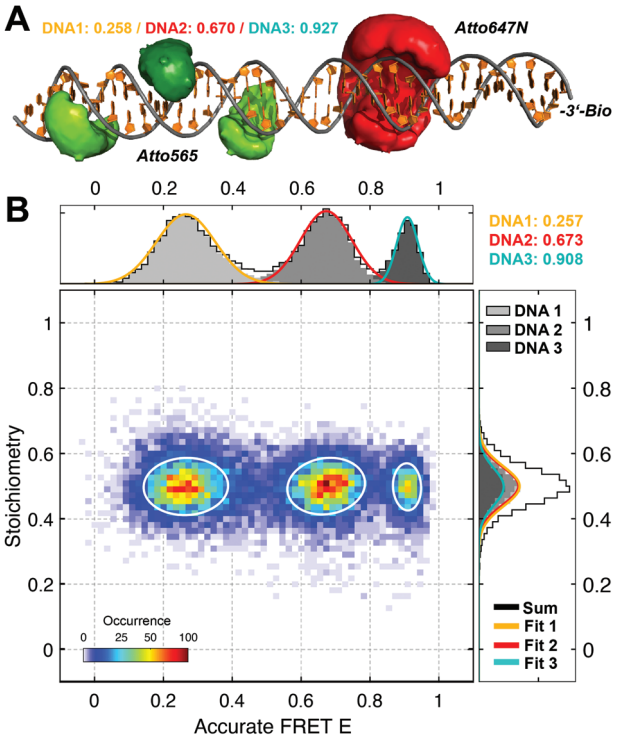

Figure 5. Characterization of dsDNA oligonucleotides serving as FRET standards. A) Depiction of location of the donor and acceptor fluorophores using an AV simulation on double-labeled dsDNA. The red and green clouds along the helix mark the accessible positions of the acceptor Atto647N (base pair 27, top strand) and donor Atto565 (base pair 6, 12, 18 on the bottom strand), respectively. The expected FRET efficiencies from the AV simulations are 0.258, 0.670, and 0.927 for the low, middle, and high FRET constructs respectively. B) An accumulative stoichiometry versus FRET efficiency plot of the three dsDNA constructs. Accurate FRET efficiencies of 0.257, 0.673, and 0.908 were determined for the FRET constructs.

According to the AV calculations, the theoretical FRET values for the three FRET constructs are 0.258 (DNA1; low), 0.670 (DNA2; middle), and 0.927 (DNA3; high). Figure 5B shows the obtained, accurate FRET histograms of each species with efficiencies of 0.257, 0.673, and 0.908. The predicted and measured values are in excellent agreement (**Table 1**).

3.3.2. Correlated 3D FRET-Tracking Experiments

Having calibrated the dsDNA constructs with MFD-PIE, we then measured the FRET state of dsDNAs attached to beads diffusing in solution using 3D orbital tracking. For this modality, a four-orbit excitation/detection scheme was used

Table 1. FRET values obtained from 3D Orbital Tracking, MFD-PIE experiments, and AV Simulations.

R_0 = 68 [Å]	FRET Efficiency	3D OT	3D OT (altern.)	PIE-MFD	AV Simulation
Gamma γ	—	**1.37**	**0.7**	**0.61**	—
DNA 1	Low	0.151	0.257	0.257	0.258
DNA 2	Middle	0.473	0.631	0.673	0.670
DNA 3	High	0.632	0.806	0.908	0.927

(Figure 2E): 1) tracking orbit (488 nm excitation) with position update, 2) the emission readout after acceptor excitation to probe the presence and photophysical state of the acceptor fluorophore (633 nm excitation) with no position update, 3) tracking orbit with repositioning (488 nm excitation) and 4) the FRET readout, i.e., dual-color emission after donor excitation (with 561 nm) (see Experimental Section). With this approach, we gather the diffusion information as well as spFRET data with alternating laser excitation to monitor the presence and photophysical state of the acceptor.[29,37]

The trajectory of the diffusing particles (**Figure 6**A–C) showed the expected Brownian motion of the particles in solution. The determined hydrodynamic radius (≈800 nm), determined from the distribution of diffusion coefficients, is centered around ≈0.17 μm^2 s^{-1} (Figure S8A, Supporting Information) and again slower than expected. Using fluorescence correlation

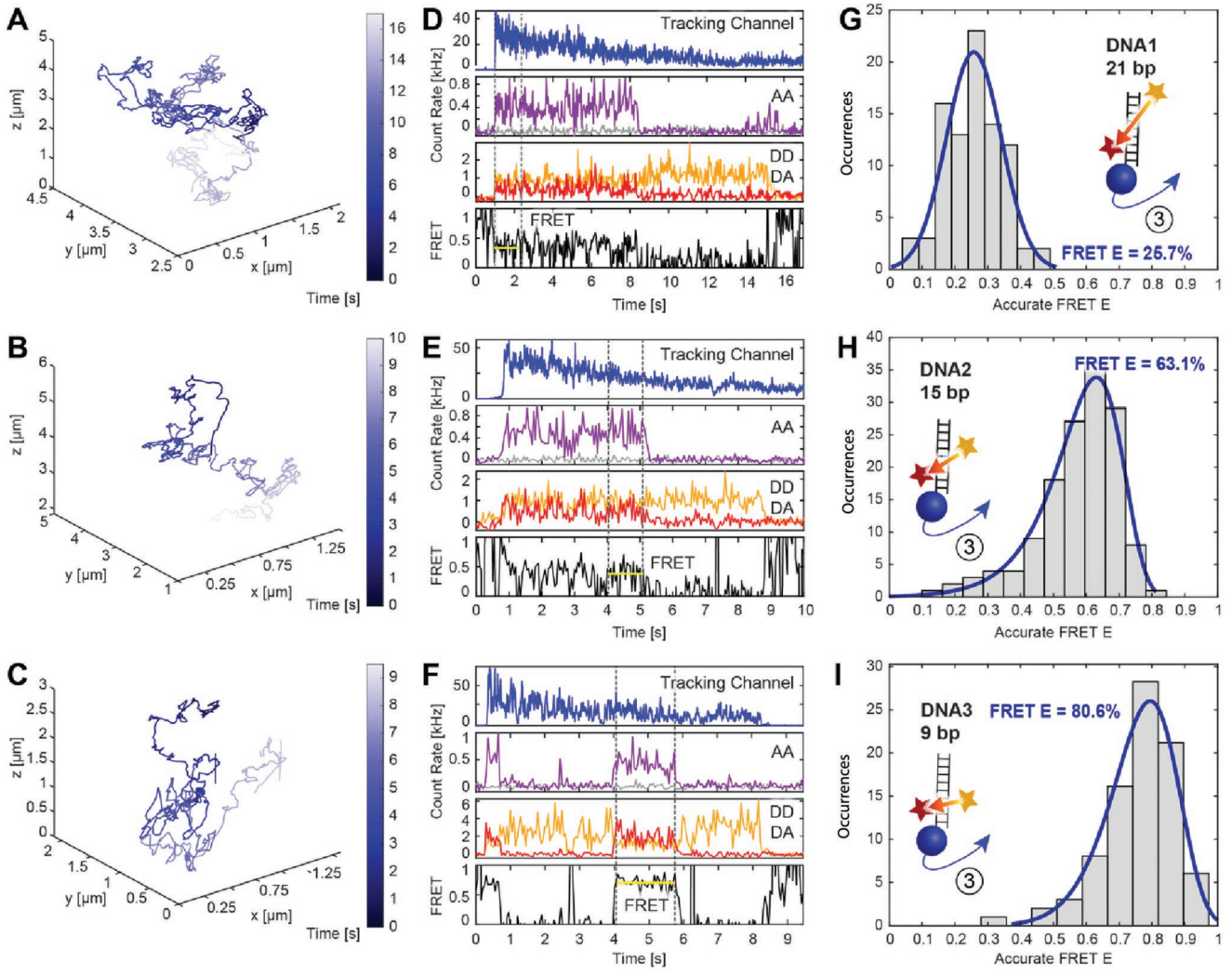

Figure 6. Single-molecule FRET measurements on diffusing DNA molecules. While tracking the reference beads marked with Atto488 dyes in solution panel (A–C), we monitored the signature of single DNA-based FRET standards panel (D–F) that were attached to the particle via a biotin-streptavidin interaction. The dsDNA oligos were double-labeled with Atto565 and Atto647N. The donor dye was positioned at three different distances with respect to the acceptor dye. The resulting oligos are characterized by a G) low FRET value of ≈26% (DNA1), H) an intermediate FRET value of 63% (DNA2), and I) a high FRET value of 81% (DNA3).

spectroscopy to study the diffusional behavior of the Atto488-labeled silica beads alone (Figure S8B, Supporting Information), we could confirm these results and further show that labeled particles dispersed in imaging buffer also tend to aggregate as seen from the tail at long lag times. This increased particle size due to the protein corona and glycerol was further observed in DLS experiments (Figure S9, Supporting Information). In addition, SEM reveals a substantial contribution of non-spherical joint silica particles with an extended length between 400 and 700 nm (Figure S10, Supporting Information), which would decrease the measured diffusion coefficient. Given the variety of characterization methods and sensitivities, these findings highlight the strength of our 3D Orbital tracking approach, which provides a direct readout on the diffusional properties of the individual particles being tracked.

The corresponding fluorescent intensities for the particles measured in Figure 6A–C are shown in Figure 6D–F. The blue intensities correspond to the tracking channel, the purple signal to acceptor emission after 633 nm excitation (ALEX channel or AA channel), and the orange (DD channel) and red intensities (DA channel) correspond to the Atto565 (donor) and Atto647N (acceptor) signal after donor excitation, respectively. As seen in Figure 6D–F, the Atto488 signal in the tracking channel comes from ≈25 to 30 Atto488 molecules (estimated using an average brightness of 1.5 kHz per emitter) that are photobleaching over time while tracking the motion of the bead. The donor and acceptor signal intensities were examined from experiments where single-step photobleaching events were observed. These traces and those exhibiting a similar intensity range were further analyzed. This ensured that only a single dsDNA was present on the bead. The signals were then background corrected for Rayleigh scattering of the laser light, estimated from beads not containing dsDNA strands, and further corrected for direct excitation ($\alpha = 0.47$), spectral cross talk ($\beta = 0.21$) and the detection efficiency γ.[29,37–39] The correction against direct excitation and spectral cross talk (see Material Section) could be reliably carried out by applying the mean values $\overline{\alpha}$ and $\overline{\beta}$ to all recorded FRET traces (Figure S11A,B, Supporting Information).

Determination of the detection correction factor $\overline{\gamma}$, however, is more challenging. The obtained γ values are particle-dependent and varied between 0 and 4 with an average value of 1.37 (determined from acceptor photobleaching steps, Figure S11C, Supporting Information). However, this value is too large for the filters used in the instrument and leads to an underestimation of the FRET values by 15–30%. The difficulties in determining γ are due to several factors. Chromatic aberrations and geometric mismatch of the excitation volumes lead to biases in the detection efficiency and thus to a position-dependent γ factor. Scattering from the bead to which the dsDNA is attached depends on the position of the particle in the orbit as well as the size and morphology of the bead. Hence, correct subtraction of the scattering for the individual beads is challenging. Moreover, in contrast to PIE/nsALEX[33,40] and µsALEX[37] single-molecule experiments, the 5 ms alternating timescale of moving objects leads to a broadening of the measured stoichiometry value, which makes it unusable for the determination of the detection correction factor $\overline{\gamma}$.[29]

As an alternative, we used the γ factor from the MFD-PIE instrument, which incorporates very similar filters and detectors ($\overline{\gamma}$ = 0.7. Table 1). Using this detection correction factor, we obtained values of 25.7%, 63.1%, and 80.6% for the low, intermediate, and high FRET constructs. The low and intermediate FRET values are well in line with the MFD-PIE data and the expected results from AV simulations. The high FRET efficiency value deviates more than it should but is clearly distinguishable from the other two constructs.

4. Discussion

By expanding the number of fluorescence species that can be tracked at a time, the amount of information collected in a single experiment can be greatly enhanced. Using a second detection channel, 3D orbital tracking is capable of following the position and thereby distance between two spectrally distinct particles either independently or within the vicinity of one of the species. In addition, the second channel can also be used for performing spectroscopy (spFRET in this case) on the tracked particle.

In the first mode, we were able to track both particles independently with separations of over 20 µm. Other recently published dual-color approaches are only able to track two particles when they are within the detection volume of the microscope.[23,24] From the 3D trajectories, the typical information such as the hydrodynamic radius of individual particles and diffusional kinetics can be monitored with time. However, the independent, dual-color tracks were generally restricted to shorter measurement times before being lost by the setup due to the repositioning of the optical devices. In particular, the piezo stage for the objective used to follow the z motion of the particle has a response time on the ≈10 ms timescale.

In the current configuration, the system is capable of robustly tracking molecules with diffusion coefficients up to ≈1–2 µm^2 s^{-1}. For a diffusion coefficient of 1 µm^2 s^{-1}, there is a 0.2% chance of the particle moving ≥500 nm (out of the orbit radius) within 10 ms, in which case the microscope will lose the particle in the lateral direction. The piezo stage used for moving the objective is the element in the system that limits the overall 3D tracking speed. Hence, the particle will be lost after a few seconds (Figure S12, Supporting Information). When tracking a single particle, it is only necessary to move the objective by the distance the particle has moved in z. However, when independently tracking two particles, the objective needs to oscillate between the two different z positions. With the slow response time of the piezo combined with our orbit time of 5 ms, the system in its current implementation has difficulties following rapidly diffusing particles in three dimensions for long periods of time. This could be improved by replacing the piezo with an electronically tunable lens, as has been shown by Annibale et al.[41] Replacing a piezo nanopositioner with an electronically tunable lens for z-tracking in 3D orbital tracking has led to more than a tenfold increase in response time of the system. In this configuration, one could consider replacing the water objective with a high NA oil objective to collect more photons as the objective is not moving during tracking.

When one is not pushing the temporal limits of the system, multiple orbits can be performed on each particle to properly "lock-in", which would decrease the fluorescence fluctuations observed during tracking (e.g., in Figure 4A). However, the position of the particle is determined from the modulation of the signal during the orbit and the difference in intensity between the different z-planes. Hence, the tracking precision is much less affected by the fluctuations in intensity.

We would like to mention that the microscope was designed for measuring processes in live cells or organisms.[12,15] To demonstrate this, we followed the endocytosis of "purple" fluorescent silica beads in HuH7 cells (**Figure 7**A). Figure 7B shows the trajectory of a bead uptaken by an early endosome and its

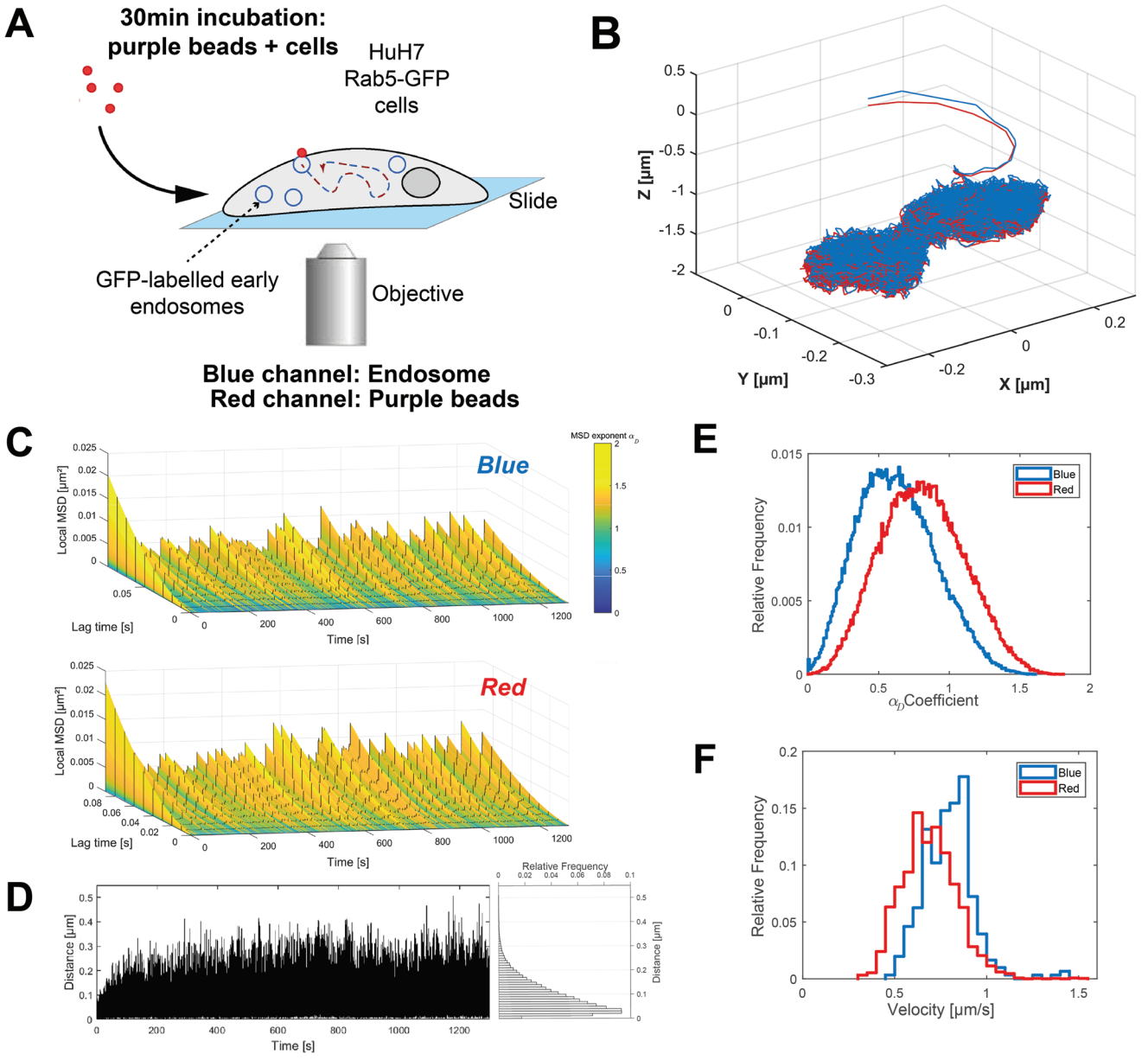

Figure 7. Long-duration dual-color tracking of a bead during endocytosis. A) The principle of the experiment: polystyrene beads (Red, 633 nm laser excitation) are incubated with HuH7 cells expressing the fluorescently tagged marker Rab5-GFP for early endosomes (blue, 488 nm laser excitation) at room temperature. B) The corresponding trajectory is represented as a 3D plot showing a fast uptake followed by transport and diffusion within the cytosol over 22 min. C) The corresponding MSD plots obtained along the trajectory using a sliding window are plotted in 3D. The values of the α_D-coefficient calculated with the equation (Equation 8) are encoded in color. The value characterizes the type of diffusion the particles exhibit: an α_D -coefficient <1 indicates sub-diffusion, ≈1 for random diffusion, and >1 super-diffusion. Each value was determined by fitting the MSD function for every time point t. D) The chromatically corrected distances between the two particles were calculated along the trajectory as a function of time. A relative frequency histogram is plotted to the right. E) The distribution of α_D-coefficients is shown for the bead in red and the endosome in blue. F) For regions containing $\alpha_D > 1.4$, we plot the distribution of extracted velocities (See Experimental Section for details). The velocities are between 0.5 and 1 µm s^{-1}, which is a typical range for transport processes in cells.

transport within the endosome through the cell. The trajectory was collected over >20 min yielding more than 120,000 data points that were analyzed in both channels. By performing a sliding window MSD analysis along the trajectory, we could identify regions of directed transport interspersed with pauses or random motion (Figure 7C). We also investigated the separation between the position of the endosome and the bead (Figure 7D). The typically separation is ≈20 nm with occasional fluctuations to larger distances. As we expect the two objects to colocalize, the separation of 20 nm can be interpreted as an upper limit of the precision of the independent tracking modality in a living cell. The distribution of determined exponent, α_D, and the velocities during transport are shown in Figure 7E,F (see Experimental Section for details). This provides a glimpse of the type of information the two-color, 3D orbital tracking system can provide in a cellular environment.

For most biological processes in living cells, the response time of the system is sufficient. In addition, the axial travel range of objects in cells tends to be limited.

For determination of the z position, we split the observation into two planes. As for any bi-plane technique, this leads to a trade off in photons detected in each focal plane for increased temporal resolution. Alternatively, one can oscillate the objective and measure orbits above and then below the laser focus, as has been done previously using 2-photon excitation.[14] For determination of the x and y position, we sum the photons from both detectors together before calculating the radial position. Hence, the loss of sensitivity for x-y detection is minimal. Unfortunately, there is currently no convenient and efficient way of separating photons being emitted from two focal planes spaced ≈200 nm apart.

In the second mode, one spectral channel can be used for tracking while the fluorescence of another species is probed during alternating orbits. This improves the robustness of tracking algorithm while the instrument is focused on following a single particle and not jumping between locations. This modality is similar to the extended TSUNAMI approach[23] with similar precision, and the spatial distance between both species encodes information regarding conformational changes of the tracked particle. For our system, there were no conformational changes and the distance was constant as expected.

By modifying the second tracking channel and the data collection software, we could successfully combine 3D orbital tracking experiments with single-molecule-sensitive FRET detection. In contrast to the tetrahedral approach,[24] by alternating the corresponding laser lines and our novel detection algorithm, we could determine the FRET correction factors of the species and thereby calculate an accurate FRET efficiency. For the very high-FRET construct, we did have discrepancies in the determined accurate FRET value. Measuring accurate FRET when the dyes are in very close proximity is very tricky. First of all, the signal from the donor fluorophore is low and accurate correction of the background signal is necessary for an accurate estimation of the FRET efficiency. At short distances, other phenomena such as Dexter transfer or dye-dye quenching can influence the FRET measurement. In addition, as we already discussed, the 10 ms delay between the FRET and the ALEX measurements biases the calculation of the correction factor for detection efficiency.

The three modalities united within one single setup represent an advanced and biophysical tool that opens the possibility to monitor the interaction of freely diffusing reaction partners, such as an endosome on a microtubule. In addition, spFRET can be accurately measured on an actively tracked object.

Supporting Information

Supporting Information is available from the Wiley Online Library or from the author.

Acknowledgements

The authors are indebted to Christoph Zimmermann from the group of Olivia Merkel for assisting with dynamic light scattering experiments and Benjamin März from the laboratory of Knut Müller–Caspary for collecting the electron microscopy images. The authors thank Dr. Nadia Ruthardt for providing the HuH7 Rab5-GFP cell lines. The authors gratefully acknowledge the financial support from the Deutsche Forschungsgemeinschaft (DFG, German Research Foundation) – Project-ID 201269156 – SFB 1032 Project B03 to D.C.L. and PL 696/4-1 to E.P. and funding by the Federal Ministry of Education and Research (BMBF) and the Free State of Bavaria under the Excellence Strategy of the Federal Government and the Länder through the ONE MUNICH Project Munich Multiscale Biofabrication. The authors also thankfully acknowledge the support of the Excellence Clusters Nanosystems Initiative Munich (NIM) and the LMU via the Center of NanoScience Munich (CeNS) and the LMU innovative BioImaging Network. F.M. and D.C.L. are eternally indebted to the coffee machine.

Open access funding enabled and organized by Projekt DEAL.

Conflict of Interest

The authors declare no conflict of interest.

Author Contributions

The project was conceived by and carried out under the supervision of D.C.L. F.W. added a second detection channel to the 3D orbital tracking microscope. F.M. programmed the data acquisition and data evaluation software, designed the bead assay, and carried out the tracking experiments in vitro. E.P. designed, prepared, and characterized the FRET standards using PIE-MFD and performed accessible volume calculations and DNA simulations. V.R. designed the in cellulo assay, carried out the associated tracking experiment and characterized the beads using FCS. F.M., E.P., V.R. and D.C.L. analyzed and interpreted the data. F.M., V.R. and E.P. designed the figures. F.M., E.P., V.R. and D.C.L. wrote the manuscript.

Data Availability Statement

The data that support the findings of this study are available from the corresponding author upon reasonable request.

Keywords

active feedback tracking, dual-color tracking, Forster resonance energy transfer (FRET), real-time three-dimensional (3D) single particle tracking, single molecule spectroscopy

Received: August 2, 2022
Revised: December 23, 2022
Published online: January 29, 2023

[1] H. C. Berg, *Rev. Sci. Instrum.* **1971**, *42*, 868.
[2] S. Ram, D. Kim, R. J. Ober, E. S. Ward, *Biophys. J.* **2012**, *103*, 1594.
[3] M. Speidel, A. Jonáš, E.-L. Florin, *Opt. Lett.* **2003**, *28*, 69.
[4] S. R. P. Pavani, M. A. Thompson, J. S. Biteen, S. J. Lord, N. Liu, R. J. Twieg, R. Piestun, W. E. Moerner, *Proc. Natl. Acad. Sci. USA* **2009**, *106*, 2995.
[5] Y. Shechtman, L. E. Weiss, A. S. Backer, S. J. Sahl, W. E. Moerner, *Nano Lett.* **2015**, *15*, 4194.
[6] G. A. Lessard, P. M. Goodwin, J. H. Werner, *Appl. Phys. Lett.* **2007**, *91*, 224106.
[7] E. P. Perillo, Y.-L. Liu, K. Huynh, C. Liu, C.-K. Chou, M.-C. Hung, H.-C. Yeh, A. K. Dunn, *Nat. Commun.* **2015**, *6*, 7874.
[8] S. Hou, J. Exell, K. Welsher, *Nat. Commun.* **2020**, *11*, 3607.
[9] F. Balzarotti, Y. Eilers, K. C. Gwosch, A. H. Gynnå, V. Westphal, F. D. Stefani, J. Elf, S. W. Hell, *Science* **2017**, *355*, 606.
[10] L. A. Masullo, F. Steiner, J. Zähringer, L. F. Lopez, J. Bohlen, L. Richter, F. Cole, P. Tinnefeld, F. D. Stefani, *Nano Lett.* **2021**, *21*, 840 .
[11] C. Hellriegel, E. Gratton, *J. R. Soc., Interface* **2009**, *6*, S3.
[12] F. Wehnekamp, G. Plucińska, R. Thong, T. Misgeld, D. C. Lamb, *Elife* **2019**, *8*, e46059.
[13] J. Enderlein, *Appl. Phys. B* **2000**, *71*, 773.
[14] V. Levi, Q. Ruan, K. Kis-Petikova, E. Gratton, *Biochem. Soc. Trans.* **2003**, *31*, 997.
[15] I. Verdeny-Vilanova, F. Wehnekamp, N. Mohan, Á. S. Álvarez, J. S. Borbely, J. J. Otterstrom, D. C. Lamb, M. Lakadamyali, *J. Cell Sci.* **2017**, *130*, 1904.
[16] F. Begarani, F. D'autilia, G. Signore, A. Del Grosso, M. Cecchini, E. Gratton, F. Beltram, F. Cardarelli, *ACS Nano* **2019**, *13*, 1670.
[17] M. Gabriel, A. Anzalone, E. Gratton, L. C. Estrada, *Microsc. Res. Tech.* **2019**, *82*, 1835.
[18] K. McHale, H. Mabuchi, *J. Am. Chem. Soc.* **2009**, *131*, 17901.
[19] Y. Yu, Y. Gao, Y. Yu, *ACS Nano* **2018**, *12*, 11871.
[20] Y. Ding, C. Li, *Biomed. Opt. Express* **2016**, *7*, 4187.
[21] D. Albrecht, C. M. Winterflood, H. Ewers, *Methods Appl. Fluoresc.* **2015**, *3*, 024001.
[22] K. Kis-Petikova, E. Gratton, *Microsc. Res. Tech.* **2004**, *63*, 34.
[23] Y.-L. Liu, E. P. Perillo, P. Ang, M. Kim, D. T. Nguyen, K. Blocher, Y.-A. Chen, C. Liu, A. M. Hassan, H. T. Vu, Y.-I. Chen, A. K. Dunn, H.-C. Yeh, *ACS Nano* **2020**, *14*, 7927.
[24] A. M. Keller, M. S. Devore, D. G. Stich, D. M. Vu, T. Causgrove, J. H. Werner, *Anal. Chem.* **2018**, *90*, 6109.
[25] V. Kudryavtsev, M. Sikor, S. Kalinin, D. Mokranjac, C. A. M. Seidel, D. C. Lamb, *ChemPhysChem* **2012**, *13*, 1060.
[26] F. Mieskes, F. Wehnekamp, G. Plucińska, R. Thong, T. Misgeld, D. C. Lamb, *Data Brief* **2020**, *29*, 105280.
[27] N. Al Danaf, Ph.D. Thesis, *Advanced Fluorescence Methodologies for the Exploration of the Nanoworld*, Ludwig-Maximilians-Universität München, Germany, **2021**.
[28] A. Dupont, M. Gorelashvili, V. Schüller, F. Wehnekamp, D. Arcizet, Y. Katayama, D. C. Lamb, D. Heinrich, *New J. Phys.* **2013**, *15*, 075008.
[29] N. K. Lee, A. N. Kapanidis, Y. Wang, X. Michalet, J. Mukhopadhyay, R. H. Ebright, S. Weiss, *Biophys. J.* **2005**, *88*, 2939 .
[30] W. Schrimpf, A. Barth, J. Hendrix, D. C. Lamb, *Biophys. J.* **2018**, *114*, 1518.
[31] T. E. Tomov, R. Tsukanov, R. Masoud, M. Liber, N. Plavner, E. Nir, *Biophys. J.* **2012**, *102*, 1163.
[32] V. Levi, Q. Ruan, E. Gratton, *Biophys. J.* **2005**, *88*, 2919.
[33] P. Toonkool, D. G. Regan, P. W. Kuchel, M. B. Morris, A. S. Weiss, *J. Biol. Chem.* **2001**, *276*, 28042.
[34] B. K. Müller, E. Zaychikov, C. Bräuchle, D. C. Lamb, *Biophys. J.* **2005**, *89*, 3508.
[35] J. Widengren, V. Kudryavtsev, M. Antonik, S. Berger, M. Gerken, C. A. M. Seidel, *Anal. Chem.* **2006**, *78*, 2039.
[36] S. Kalinin, T. Peulen, S. Sindbert, P. J. Rothwell, S. Berger, T. Restle, R. S. Goody, H. Gohlke, C. A. M. Seidel, *Nat. Methods* **2012**, *9*, 1218.
[37] A. N. Kapanidis, N. K. Lee, T. A. Laurence, S. Doose, E. Margeat, S. Weiss, *Proc. Natl. Acad. Sci. USA* **2004**, *101*, 8936.
[38] E. Lerner, A. Barth, J. Hendrix, B. Ambrose, V. Birkedal, S. C. Blanchard, R. Börner, H. Sung Chung, T. Cordes, T. D. Craggs, A. A. Deniz, J. Diao, J. Fei, R. L. Gonzalez, I. V. Gopich, T. Ha, C. A. Hanke, G. Haran, N. S. Hatzakis, S. Hohng, S.-C. Hong, T. Hugel, A. Ingargiola, C. Joo, A. N. Kapanidis, H. D. Kim, T. Laurence, N. Ki Lee, T.-H. Lee, E. A. Lemke, et al., *Elife* **2021**, *10*, e60416.
[39] C.-B. Salem, E. Ploetz, D. C. Lamb, in *Spectroscopy and Dynamics of Single Molecules*, (Ed.: C. K. Johnson), Elsevier, Amsterdam **2019**, pp. 71–115.
[40] A. N. Kapanidis, T. A. Laurence, N. K. Lee, E. Margeat, X. Kong, S. Weiss, *Acc. Chem. Res.* **2005**, *38*, 523.
[41] P. Annibale, A. Dvornikov, E. Gratton, *Biomed. Opt. Exp.* **2015**, *6*, 2181.